AIP Applied Physics Letters

Multi-functional stacked light-trapping structure for stabilizing and boosting solar-electricity efficiency of hydrogenated amorphous silicon solar cells

Wen-Hsien Huang, Jia-Min Shieh, Fu-Ming Pan, Chang-Hong Shen, Jung Y. Huang, Tsung-Ta Wu, Ming-Hsuan Kao, Tzu-Hsuan Hsiao, Peichen Yu, Hao-Chung Kuo, and Ching-Ting Lee

Citation: Applied Physics Letters **103**, 073107 (2013); doi: 10.1063/1.4818621
View online: http://dx.doi.org/10.1063/1.4818621
View Table of Contents: http://scitation.aip.org/content/aip/journal/apl/103/7?ver=pdfcov
Published by the AIP Publishing

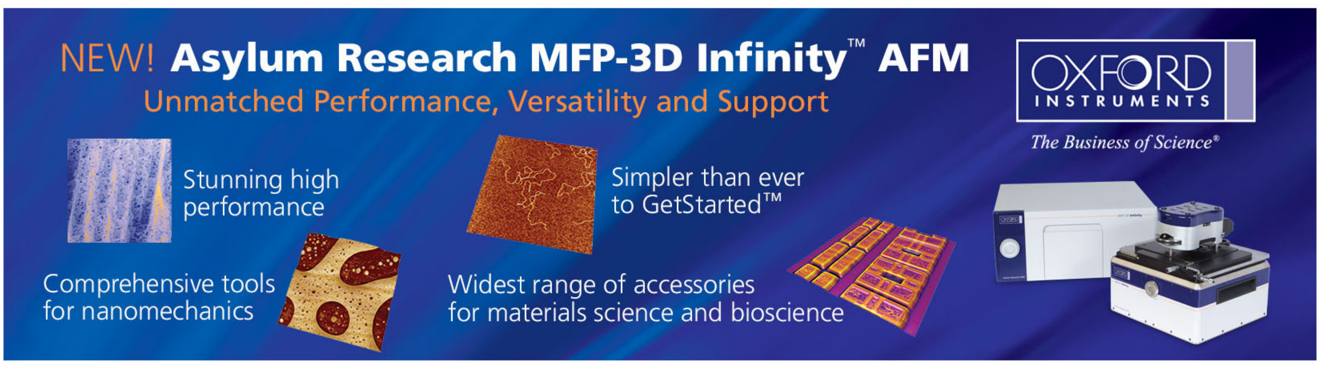

APPLIED PHYSICS LETTERS 103, 073107 (2013)

Multi-functional stacked light-trapping structure for stabilizing and boosting solar-electricity efficiency of hydrogenated amorphous silicon solar cells

Wen-Hsien Huang,[1] Jia-Min Shieh,[2,3,a)] Fu-Ming Pan,[1,b)] Chang-Hong Shen,[2] Jung Y. Huang,[3] Tsung-Ta Wu,[2] Ming-Hsuan Kao,[3] Tzu-Hsuan Hsiao,[3] Peichen Yu,[3] Hao-Chung Kuo,[3] and Ching-Ting Lee[4]

[1]*Department of Materials Science and Engineering, National Chiao-Tung University, Hsinchu 30010, Taiwan*
[2]*National Nano Device Laboratories, No. 26, Prosperity Road 1, Hsinchu 30078, Taiwan*
[3]*Departments of Photonics and Institute of Electro-Optical Engineering, National Chiao-Tung University, Hsinchu 30010, Taiwan*
[4]*Institute of Microelectronics, Department of Electrical Engineering, National Cheng Kung University, Tainan 701, Taiwan*

(Received 8 February 2013; accepted 29 July 2013; published online 13 August 2013)

A sandwiched light-trapping electrode structure, which consists of a capping aluminum-doped ZnO (AZO) layer, dispersed plasmonic Au-nanoparticles (Au-NPs), and a micro-structured transparent conductive substrate, is employed to stabilize and boost the conversion-efficiency of hydrogenated amorphous silicon (a-Si:H) solar cells. The conformal AZO ultrathin layer (5 nm) smoothened the Au-NP-dispersed electrode surface, thereby reducing defects across the AZO/a-Si:H interface and resulting in a high resistance to photo-degradation in the ultraviolet-blue photoresponse band. With the plasmonic light-trapping structure, the cell has a high conversion-efficiency of 10.1% and the photo-degradation is as small as 7%. *© 2013 AIP Publishing LLC*. [http://dx.doi.org/10.1063/1.4818621]

Hydrogenated amorphous silicon (a-Si:H) thin film solar cells have attracted a wide attention because of their low-cost and low-thermal budget characteristics. To maximize the photoconversion efficiency of a solar cell, one needs to improve photo-absorption, photocurrent generation, and carrier-collection for the cell; these can be realized by optimization of the cell structure, including band-gap-engineered active layers of low defect, highly transparent conductive metal-oxide (TCO) layers with a micro-structured texture or multi-scale-structure,[1,2] and the introduction of plasmonic nanoparticles (NPs).[3] However, textured transparent electrodes barely provide multi-functionalities and efficient carrier collection for broadband light-trapping structures. Moreover, they are not suitable substrates for stacking multi-layered photovoltaic devices of high quality. A front-side ZnO electrode with a three-dimensional hexagonal micro-hole array, which was patterned by electron beam lithography, has been demonstrated to enhance the conversion efficiency of micromorph Si-based thin-film solar cells. The optical modeling shows that a-Si:H/μc-Si:H micromorph cells with the micro-hole array electrode can achieve a conversion efficiency of 15%. However, experimental result yields a conversion efficiency of only 10.3%.[4] Boccard *et al.*, recently reported a new broadband light-trapping architecture that produced a conversion efficiency of 14.1% for micromorph solar cells.[1,2] The front-side electrode of the trapping structure had a homogeneous multi-scale ZnO layer prepared by the combination of nano-imprint technique and low pressure chemical vapor deposition (CVD). In addition, when metal nano-structures[5,6] or metal NPs,[3] such Ag and Au, are combined with a thick ZnO layer for the use as the back-reflector, back light-scattering is strongly enhanced. Such nanostructures can avoid the generation of extra interface and bulk defects in a-Si:H multilayers. However, substrate-type (n-i-p) single junction solar cells fabricated with these light-trapping schemes exhibit a low conversion efficiency (<8.5%). In our previous study, highly UV-transparent dielectric particles can scatter the sunlight into the a-Si:H layer mainly via the waveguide mode,[7,8] enhancing light absorption in the ultraviolet-visible wavelengths regime and, thus, raising the conversion efficiency to 8.5%.[9] For superstrate-type (p-i-n) solar cells, the incorporation of metal nano-structures or metal NPs is rarely used in the front-side light-trapping scheme for the fabrication of stable Si thin-film solar cells with high conversion efficiencies. This is because the plasmonic enhancement in the quantum efficiency (QE) occurs only in a narrow bandwidth and the formation of interface structural defects between a-Si:H absorptive layer and TCO is inevitable.[10–13] In this letter, we propose a sandwiched light-trapping structure, which consists of a capping aluminum-doped ZnO (AZO) thin film, dispersed plasmonic Au nanoparticles (Au-NPs), and a micro-structured transparent conductive electrode (Asahi SnO_2:F, FTO). Such the sandwiched structure provides the immunity to metal diffusion and a low-defect AZO/a-Si:H interface, where the AZO acted as a protective layer eliminating H^+ ion bombardment on the electrode substrate.[14] The low plasma power density for the a-Si:H deposition can also minimize the ion bombardment on the substrate.[15] Moreover, the nano-scale smooth surface of the TCO electrode by smoothening the protrusion and sharp valley of FTO/Au-NPs is beneficial to the growth of the dense a-Si:H film of low-defect density.[16] The Au-NPs/AZO layer enhances the absorption of the green-red solar energy via the plasmonic effect, and the micro-structured FTO functions like a short-wavelength scatter, which increases the ultraviolet-blue solar-energy utilizaiton.[1] Because of these merits, the sandwich structure enhances

a)E-mail: jmshieh@ndl.narl.org.tw (or jmshieh@faculty.nctu.edu.tw). Tel.: 886-3-5726100-7617. Fax: 886-3-5722715
b)E-mail: fmpan@faculty.nctu.edu.tw. Tel.: 886-3-5712121-31322. Fax: 886-3-5724727

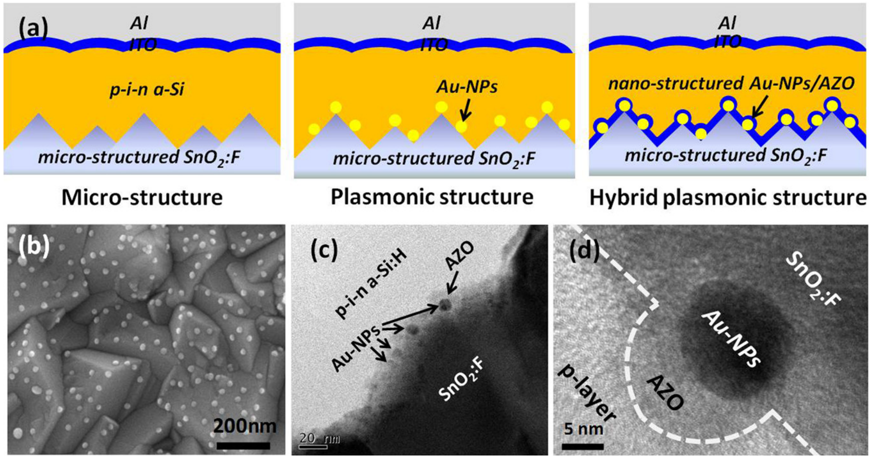

FIG. 1. (a) The schematic diagram of p-i-n-type a-Si:H thin film solar cell for micro-structured electrode of FTO (MS), plasmonic-structured electrode of FTO/Au-NPs (PS) and FTO/Au-NPs/AZO hybrid electrode (HPS); (b) 15 nm Au-NPs self-assembled on FTO electrode; (c) the cross-sectional TEM image of p-i-n-type a-Si:H thin film solar cells on HPS electrode; (d) the HRTEM image across FTO, Au-NPs, AZO, and a-Si:H p-layer.

broadband light-harvesting and reduce the defect density across the AZO/a-Si:H interface for the a-Si:H thin film solar cell that demands a high conversion efficient and high resistance to photo-degradation. The solar cell integrated the sandwich scheme with the low-defect a-Si:H stacked layer[16] exhibits a short circuit current density (J_{sc}) of 16.6 mA/cm^2, filling factor (FF) of 72.4%, conversion efficiency (η) of 10.1%, and high resistance to photo-degradation (<7%).

The fabrication of the a-Si:H solar cell begins with the preparation of the multi-functional front-side electrode. First Au-NPs were self-assembled on the micro-structured Asahi-type substrate (SnO_2:F, FTO), followed by the deposition of an ultra-thin AZO capping layer. The a-Si:H p-i-n multilayer (12-nm p-layer/400-nm i-layer/20-nm n-layer) was then deposited on the light-trapping electrode by high-density inductively coupled plasma CVD (ICP-CVD),[15] which can produce a-Si:H thin-films of low defect at the substrate temperature of 140 °C. A 80-nm-thick indium tin oxide (ITO) and a 500-nm-thick Al metal were then deposited on the ICP a-Si:H p-i-n multilayer as the back-electrode. The monodispersed Au-NPs of 15 nm in size in water solution were synthesized by the citrate chemical reduction method at low temperatures.[17] To form the self-assembled Au-NPs monolayer on the micro-textured FTO substrate, we sequentially immersed the bare FTO-covered glass substrate in the 3-aminopropyltrimethoxysilane (APTMS)/ethanol solution and the solution containing dispersed Au-NPs. The APTMS forms strong chemical bonds with FTO and can selectively attach to Au-NPs via the terminal ligand (-C-NH_3). The deposition of the conformal AZO capping layer (5 nm) on the self-assembled Au-NPs monolayer was carried out using scanning-mode DC-sputtering deposition, which was operated at a low power density (0.75 W/cm^2), a low pressure (2.4 mTorr), and a low scanning speed (6 mm/s) to reduce the deposition rate (2 A/s). The FTO substrate without Au-NPs was used as the control sample. The photovoltaic performance was characterized by an AM1.5G Global sun simulator (Oriel Sol3A) with the white light of 1000 W/m^2 irradiance. The light-soaking measurement was performed under the white-light irradiance of 6000 W/m^2 (6-Sun). The device reached accordingly a steady-state temperature at 60 °C due to the irradiation, thereby accelerating photo-degradation of the device.[15] The defect density of the intrinsic a-Si:H layer on different electrodes was determined by the drive-level capacitance profiling (DLCP).[18,19]

Figure 1(a) schematically shows three structures of the p-i-n a-Si:H thin film solar cell; one is with the micro-structured FTO electrode (MS), one with the FTO/Au-NPs plasmonic electrode (PS), and one with the FTO/Au-NPs/AZO hybrid electrode (HPS). The SEM image of Fig. 1(b) shows that Au-NPs of 15 nm in size are well dispersed on the FTO substrate with the NPs density of $\sim 2 \times 10^{10}$ cm^{-2}. Excessive Au-NPs can reduce light absorption of the active layers and may result in a non-conformal AZO capping, which may induce microstructure defects, such as cracks or voids, across the AZO/a-Si:H interface. Figures 1(c) and 1(d) show the cross-sectional transmission electron microscopy (TEM) images of the p-i-n a-Si:H thin film solar cell with the FTO/Au-NPs/AZO structure. The conformal AZO layer tends to smoothen the Au-NPs dispersed FTO electrode, and microstructural defects are absent across the AZO layer, the p-layer and the intrinsic a-Si:H layer.

The current-voltage (I–V) characteristics of the a-Si:H thin film solar cells integrated with different front-side light-trapping electrodes are shown in Fig. 2. Table I lists the photovoltaic characteristics of the three light-trapping-structured solar cells. According to our previous study, the ICP intrinsic a-Si:H layer has a low-defect density of 3×10^{15} cm^{-3}.[15,19] The MS-PV shows a high J_{sc} of 16.3 mA/cm^2 with the conversion efficiency as high as 9.6%. In addition, the device has a low dark saturation current of 1.2×10^{-9} A/cm^2 and a high FF of 70.4%. When plasmonic Au-NPs are deposited on the micro-structured FTO electrode (PS-PV), the solar cell shows a degraded photovoltaic performance with $J_{sc} = 15.5$ mA/cm^2, FF = 67.8%, and $\eta = 8.85\%$. On the other hand, the insertion of the AZO layer between the p-layer and

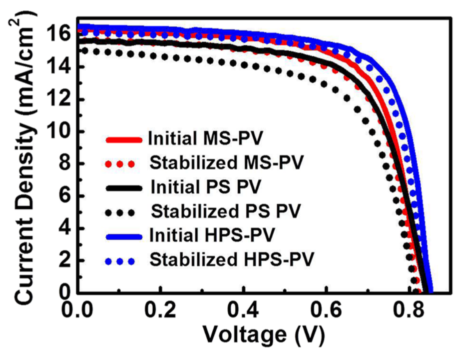

FIG. 2. The I-V characteristics of MS-, PS-, and HPS-PV devices before (initial state) and after (stabilized state) light-soaking.

TABLE I. The cell-performances comparison for the MS-, PS-, and HPS-PVs before (initial state) and after (stabilized state) light-soaking test. The cell area is 1 cm^2.

Cell type	V_{oc} (volt)	FF (%)	J_{sc}(mA/cm^2)	η (%)
MS-PV (initial state)	0.84	70.4	16.3	9.6
MS-PV (stabilized state)	0.83	62.6	15.9	8.4
PS-PV (initial state)	0.84	67.8	15.5	8.85
PS-PV (stabilized state)	0.82	62.0	15	7.65
HPS-PV (initial state)	0.84	72.4	16.6	10.1
HPS-PV (stabilized state)	0.84	68.3	16.3	9.4

the Au-NPs dispersed FTO electrode leads to an increase in the FF (72.4%) and J_{sc} (16.6 mA/cm^2), thereby greatly enhancing the conversion efficiency of the HPS-PV cell to 10.1%. The improved FF of the HPS-PV cell may be attributed to the more stable AZO/a-Si:H interface in comparison with the PS-PV cell. Because of the stable interface, the HPS-PV cell is less vulnerable to photo-degradation and, therefore, exhibits a higher conversion efficiency after light-soaking (stabilized state) as to be discussed later.

Figure 3(a) shows the initial QE spectra of the three PV cells before light-soaking. The QE of the PS-PV cell is lower in the range of 350–500 nm than that of the MS-PV cell. However, with the conformal AZO capping layer on Au-NPs, the QE of the HPS-PV cell is comparable to that of the MS-PV cell in the ultraviolet-blue band. The lower QE of the PS-PV cell in the ultraviolet-blue band is likely due to the optical loss and microstructural defects induced by Au-NPs. However, the presence of the AZO capping layer reduces the microstructural defects at the AZO/a-Si:H interface and compensates the photocurrent loss via the stable interface. Moreover, by properly adjusting the size and density of Au-NPs, and the dielectric constant of the surrounding media, one can match the localized surface plasmon resonance (LSPR) wavelength of metal-NPs in a hybrid plasmonic light-trapping structure with the specific photoresponse band of an a-Si:H PV device.[20,21] In this study, we carefully optimized the fabrication conditions of the HPS electrode, including the size and density of Au-NPs and the thickness of the AZO layer, to enhance the plasmonic effect in the green-red band. The photocurrent loss in the short wavelength range can be effectively compensated by the gain of the enhanced electromagnetic field due to the Au-NPs/AZO induced plasmonic effect. Therefore, more hole carriers are photogenerated in the active layer by the enhanced field and are extracted from the p-layer to the AZO layer, leading to a higher photocurrent in the green-red band.[11] As a result, the HPS-PV cell has a better quantum efficiency in the range of 550–650 nm than the MS-PV cell.

The reverse-bias QE method is usually employed to study the photovoltaic behavior of photogenerated carriers trapped by interface and bulk defects because the applied reverse-bias can increase the electric field across the p-i-n multilayer and, thus, enhance the extraction of photogenerated carriers. Figures 3(b)–3(d) show the QE spectra under the zero-bias (0 V) and the reverse-bias (−1 V) for the three PV devices. In a reverse-bias QE spectrum, a higher QE indicates that more photogenerated holes and electrons are trapped by defects near the p-/i-layer and the i-/n-layer interfaces, respectively.[22,23] The reverse-bias QE of the HPS-PV cell is lower in the ultraviolet-blue wavelengths regime than that of the MS-PV and PS-PV cells, suggesting a lower defect density across the interfaces. This is likely because the conformal AZO layer encourages the formation of the interface of low defect density with the intrinsic a-Si:H layer. As a result, the photocurrent loss can be compensated by a better carrier collection due to the improved microstructural property of the interface.

Figure 4(a) is the energy dispersive spectroscopy (EDS) mappings that show the elemental distribution in a selected area of the HPS-PV cell. From the mappings, Au-NPs are strictly confined in the AZO capping layer without

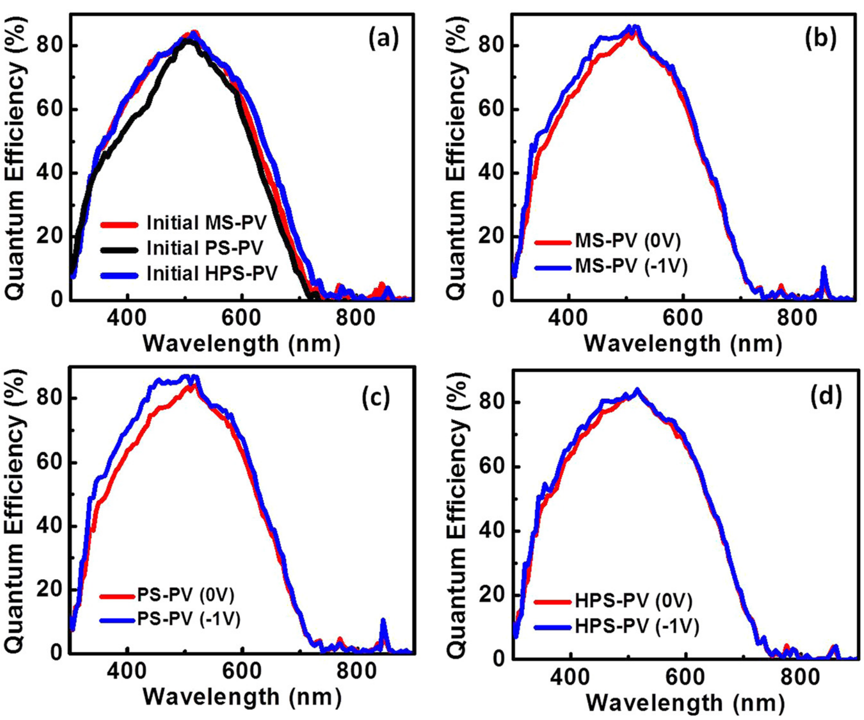

FIG. 3. (a) The initial QE of MS-, PS-, and HPS-PV devices and the QE operated under 0 V and −1 V bias for (b) MS-PV device, (c) PS-PV device, and (d) HPS-PV device.

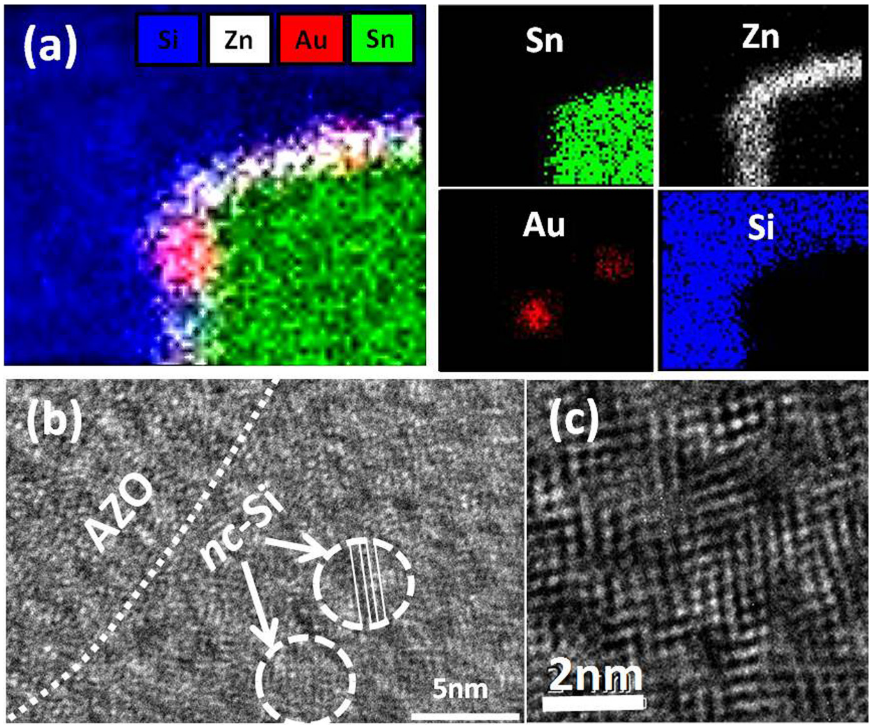

FIG. 4. (a) The elemental distribution in a selected area of the HPS-PV cell for Sn, Zn, Au, and Si by TEM-EDS, (b) the dispersed nc-Si in the a-Si:H p-layer, and (c) the inverse fast-Fourier transform image of nc-Si.

perceivable Au diffusion into the a-Si:H multilayer. The high resolution TEM (HRTEM) image in Fig. 4(b) shows the presence of crystalline Si nanograins near the interface between the p-layer and the AZO layer as indicated by the dashed circles and the inverse fast-Fourier transform image in Fig. 4(c). Raman spectroscopy also revealed the formation of nanocrystalline-Si (nc-Si) in the p-layer of the HPS-PV cell (not shown). The nc-Si grains were not found in the p-layer of the MS- and PS-PV cells, suggesting that the conformal AZO layer induces the partial crystallinity. Because the a-Si:H/nc-Si mixed-phase layer is analogous to the polymorphous Si (pm-Si) in the aspect of microstructure, it can exhibit a better photocarrier transport efficiency compared with the a-Si:H layer.[24,25]

Figure 5(a) shows the QE_{loss} of the three PV cells as a function of the light wavelength. The QE_{loss} is herein defined by the ratio of QE at -1 V to QE at 0 V. All the three cells demonstrate a higher QE_{loss} in the ultraviolet-blue wavelengths range and a lower QE_{loss} in the green-red wavelengths range, suggesting that trapped charge carriers near the p-/i-layer interface influence the photovoltaic behavior much more than those near the i-/n-layer interface.[22,23] The high QE_{loss} in the ultraviolet-blue wavelengths range primarily arises from the recombination of photogenerated electrons with holes trapped by defects near the p-/i-layer interface. Therefore, the lowest QE_{loss} of the HPS-PV cell in the ultraviolet-blue wavelengths range can be ascribed to a less hole accumulation across the p-/i-layer interface. In addition to a smaller defect density at the interface, an efficient collection of photogenerated carriers can also improve the QE_{loss}. It has been reported that the high work function of the AZO layer can moderate the abrupt band bending across the AZO/a-Si:H interface leading to a barrier height lowering and, thus, to a better collection efficiency of hole carriers.[26,27] Therefore, the introduction of the AZO layer may result in the barrier height lowering between the electrode and the p-layer and, thus, yields the better QE_{loss} of the HPS-PV cell.

To study the influence of the three transparent electrodes on the film quality of the intrinsic a-Si:H layer, we measured the bulk-defect density of the intrinsic a-Si:H layer after light illumination at 120 °C for 10^4 s by DLCP.[15,18,19] Figure 5(b) shows the integrated defect density (N_D) of the PV cells as a function of the depth from the top of the p-i-n active layer after light-soaking. The HPS-PV cell exhibits the lowest bulk-defect density of $\sim 6 \times 10^{15}\,cm^{-3}$, and both the MS- and the PS-PV cells have a N_D higher than $1.4 \times 10^{16}\,cm^{-3}$. The DLCP analysis suggests that the FTO/Au-NPs/AZO structure facilitates the growth of an intrinsic a-Si:H layer of low-defect density, which improves the stability of the HPS-PV cell after light-soaking.

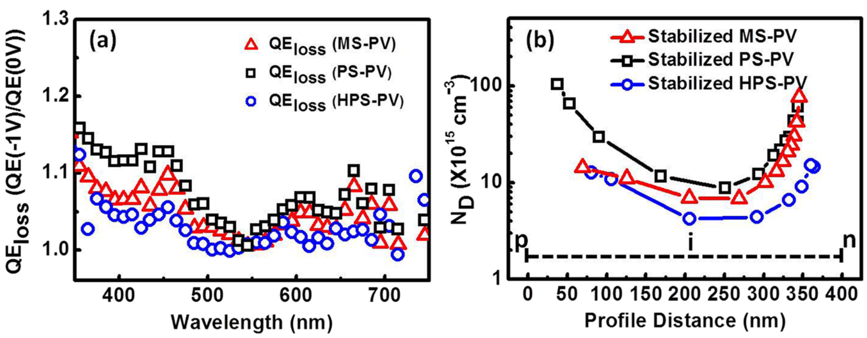

FIG. 5. (a) The normalized QE_{loss} ($QE(-1\,V)/QE(0\,V)$) of MS-, PS-, and HPS-PV devices as a function of wavelength. (b) The depth profile of bulk-defect densities in the intrinsic a-Si:H layer retrieved from DLCP measurements for MS-, PS-, and HPS-PV devices at 120 °C after 10^4-s exposure with a light irradiance of 6 Sun.

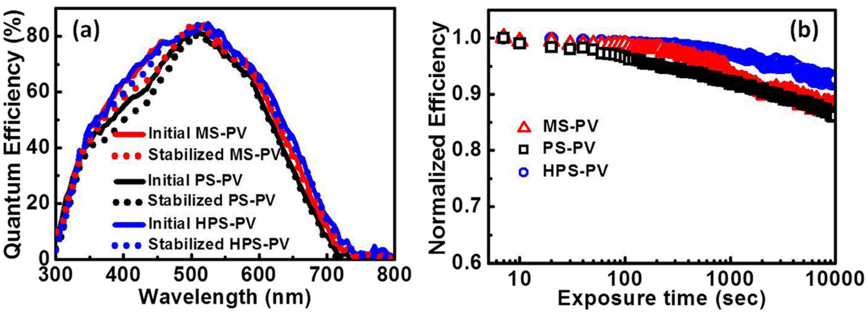

FIG. 6. (a) The QE variation of MS-, PS-, and HPS-PV devices at initial state and stabilized state, (b) the conversion efficiency degradation of MS-, PS-, and HPS-PV devices as a function of exposure time with a light irradiance of 6-Sun at 60 °C.

Photo-degradation of a-Si:H PV devices resulting from the Staebler-Wronski effect (SWE) is the major obstacle to the practical use of PV devices because the induced metastable defects during light-soaking enhances the recombination of photogenerated carriers. Figure 6(a) shows the QE spectra of the three PV cells before (initial state) and after (stabilized state) the light-soaking process. These cells demonstrate very slight photo-degradation in the green-red wavelengths range after the light-soaking. On the other hand, obvious photo-degradation occurs to all the three cells in the range of 350–500 nm. However, HPS-PV cell shows a higher resistance to photo-degradation than the MS- and PS-PV cells. Figure 6(b) shows the conversion efficiency of the PV cells subjected to light exposure of 6-sun irradiance at 60 °C as a function of the light exposure time. According to the figure and Table I, the conversion efficiency of the HPS-PV cell decreases by about 7.0% after the light exposure of 10^4 s, and the MS- and PS-PV cells show a decrease in the conversion efficiency of 12.5% and 13.6%, respectively. In combination of the hybrid plasmonic-structured electrode and the ICP-a-Si:H p-i-n multilayer of low defect density, the HPS-PV cell clearly demonstrates a high efficiency and a high stability.

In summary, the a-Si:H thin film solar cell, which consists of the hybrid plasmonic-structured AZO/Au-NPs/FTO electrode and the a-Si:H active layers of low-defect density, has a high photovoltaic efficiency and stability. The hybrid plasmonic light-trapping structure exhibits a broadband light harvest, a high conversion efficiency of 10.1% and a slight photo-degradation as small as 7% after light-soaking. The good photovoltaic properties result from the introduction of the conformal AZO ultra-thin layer between the active layers and the Au-NPs dispersed FTO substrate. The AZO layer encourages the growth of the a-Si:H layers of low defect density and, thus, improves the interface properties between the a-Si:H active layers and the electrode. As a result, the plasmonic a-Si:H solar cell has an enhanced efficiency in the green-red band and a high resistance to photo-degradation in the ultraviolet-blue wavelengths regime. This multi-functional light-trapping electrode structure has a great application potential for the a-Si:H thin film solar cell technology, in which devices of high performance and high stability are extremely desirable.

The authors thank the National Science Council of the Republic of China for financially supporting this research.

[1] M. Boccard, C. Battaglia, S. Hanni, K. Soderstrom, J. Escarre, S. Nicolay, F. Meillaud, M. Despeisse, and C. Ballif, Nano Lett. **12**, 1344 (2012).
[2] C. Battaglia, C. M. Hsu, K. Soderstrom, J. Escarre, F. J. Haug, M. Charriere, M. Boccard, M. Despeisse, D. T. L. Alexander, M. Cantoni, Y. Cui, and C. Ballif, ACS Nano **6**, 2790 (2012).
[3] X. Chen, B. Jia, J. K. Saha, B. Cai, N. Stokes, Q. Qiao, Y. Q. Wang, Z. G. Shi, and M. Gu, Nano Lett. **12**, 2187 (2012).
[4] M. Vanecek, O. Babchenko, A. Purkrt, J. Holovsky, N. Neykova, A. Poreba, Z. Remes, J. Meier, and U. Kroll, Appl. Phys. Lett. **98**, 163503 (2011).
[5] V. E. Ferry, M. A. Verschuuren, M. C. van Lare, R. E. I. Schropp, H. A. Atwater, and A. Polman, Nano Lett. **11**, 4239 (2011).
[6] J. Zhu, C. M. Hsu, Z. F. Yu, S. H. Fan, and Y. Cui, Nano Lett. **10**, 1979 (2010).
[7] M. Kroll, S. Fahr, C. Helgert, C. Rockstuhl, F. Lederer, and T. Pertsch, Phys. Status Solidi A **205**, 2777 (2008).
[8] J. Grandidier, D. M. Callahan, J. N. Munday, and H. A. Atwater, Adv. Mater. **23**, 1272 (2011).
[9] W. H. Huang, J. M. Shieh, F. M. Pan, C. H. Shen, Y. C. Lien, M. A. Tsai, H. C. Kuo, B. T. Dai, and F. L. Yang, IEEE Electron Device Lett. **33**(7), 1036 (2012).
[10] E. Moulin, J. Sukmanowski, M. Schulte, A. Gordijn, F. X. Royer, and H. Stiebig, Thin Solid Films **516**, 6813 (2008).
[11] E. Moulin, P. Q. Luo, B. Pieters, J. Sukmanowski, J. Kirchhoff, W. Reetz, T. Muller, R. Carius, F. X. Royer, and H. Stiebig, Appl. Phys. Lett. **95**, 033505 (2009)
[12] F. Lukermann, U. Heinzmann, and H. Stiebig, Appl. Phys. Lett. **100**, 253907 (2012).
[13] A. Nuruddin and J. R. Abelson, Thin Solid Films **394**, 48 (2001).
[14] N. Chantarat, S. H. Hsu, C. C. Lin, M. C. Chiang, and S. Y. Chen, J. Mater. Chem. **22**, 8005 (2012).
[15] C. H. Shen, J. M. Shieh, J. Y. Huang, H. C. Kuo, C. W. Hsu, B. T. Dai, C. T. Lee, C. L. Pan, and F. L. Yang, Appl. Phys. Lett. **99**, 033510 (2011).
[16] M. Python, O. Madani, D. Domine, F. Meillaud, E. Vallat-Sauvain, and C. Ballif, Sol. Energy Mater. Sol. Cells **93**, 1714 (2009).
[17] B. V. Enüstün and J. Trkevich, J. Am. Chem. Soc. **85**, 3317 (1963).
[18] S. Guha, J. Yang, D. L. Williamson, Y. Lubianiker, J. D. Cohen, and A. H. Mahan, Appl. Phys. Lett. **74**, 1860 (1999).
[19] J. Y. Huang, C. Y. Lin, C. H. Shen, J. M. Shieh, and B. T. Dai, Sol. Energy Mater. Sol. Cells **98**, 277 (2012).
[20] G. Xu, M. Tazawa, P. Jin, S. Nakao, and K. Yoshimura, Appl. Phys. Lett. **82**, 3811 (2003).
[21] G. Xu, Y. Chen, M. Tazawa, and P. Jin, Appl. Phys. Lett. **88**, 043114 (2006).
[22] A. E. Delahoy, A. P. Stavrides, A. M. Patel, L. T. Le, and J. A. Cambridge, Proc. SPIE **7045**, 704506 (2008).
[23] T. Soderstrom, F. J. Haug, V. Terrazzoni-Daudrix, and C. Ballif, J. Appl. Phys. **103**, 114509 (2008).
[24] P. Roca i Cabarrocas, A. Fontcuberta i Morral, and Y. Possissant, Thin Solid Films **403**, 39 (2002).
[25] L. R. Wienkes, C. Blackwell, and J. Kakalios, Appl. Phys. Lett. **100**, 072105 (2012).
[26] H. Tasaki, W. Y. Kim, M. Hallerdt, M. Konagai, and K. Takahashi, J. Appl. Phys. **63**, 550 (1988).
[27] H. S. Park, J. Y. Lee, H. W. Kim, D. Y. Kim, J. A. Raja, and J. Yi, Appl. Phys. Lett. **102**, 191602 (2013).